ACS Catalysis

Research Article

pubs.acs.org/acscatalysis

Engineering the Composition and Crystallinity of Molybdenum Sulfide for High-Performance Electrocatalytic Hydrogen Evolution

Yanpeng Li,*[,†,‡,⊥] Yifei Yu,[‡,⊥] Yufeng Huang,[§] Robert A. Nielsen,[§] William A. Goddard, III,[§] Yao Li,[†] and Linyou Cao*[,‡,∥]

[†]Center for Composite Materials and Structures, Harbin Institute of Technology, Harbin, Heilongjiang 150001, People's Republic of China

[‡]Department of Materials Science and Engineering, North Carolina State University, Raleigh, North Carolina 27695, United States

[§]Materials and Process Simulation Center, California Institute of Technology, Pasadena, California 91125, United States

[∥]Department of Physics, North Carolina State University, Raleigh, North Carolina 27695, United States

Supporting Information

ABSTRACT: The key challenge for the development of high-performance molybdenum sulfide HER catalysts lies in the limited fundamental understanding for the correlation between the catalytic activities and physical features of the materials. Here we have demonstrated an unambiguous correlation between the catalytic performance and the composition/crystallinity of molybdenum sulfide. The results indicate that the crystallinity plays an overwhelming role in determining the catalytic performance, while the composition does not matter much. The crystallinity can affect the three figures of merit of the catalytic performance (Tafel slope, turnover frequency (TOF), and stability) in opposite directions. Generally, the materials with low crystalline quality may provide low Tafel slopes (~40 mV/dec), while highly crystalline molybdenum sulfide shows higher TOFs (by 2 orders of magnitude) and better stability. DFT calculations suggest that the terminal disulfur complex S_2^{2-}, which may exist in MoS_3 and also likely MoS_2 of low crystalline quality due to its structural disorder, could be the true catalytically active site responsible for the low Tafel slope. Our results indicate that one key issue for the rational design of high-performance molybdenum sulfide HER catalysts is to engineer the crystallinity such that balancing its contradictory effects on the different aspects of the catalytic performance. We show that nanocrystalline MoS_2 with few-layer nanoclusters in a lateral size of 5−30 nm provides a more promising platform than either amorphous or highly crystalline molybdenum sulfide due to its combination of low Tafel slopes and good stability. As a way to illustrate this notion, we have developed a MoS_2 catalyst by engineering the crystallinity that shows Tafel slopes of 40 mV/dec, exchange current densities of 3.5 $\mu A/cm^2$, and extraordinary stability with constant performance over >10000 cycles, which are among the best values ever reported. The performance of this catalyst could be further improved by using rougher substrates or doping to improve the relatively low exchange current density.

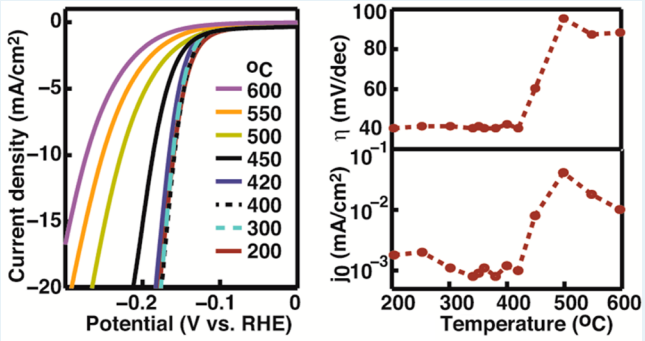

KEYWORDS: *molybdenum disulfide, molybdenum trisulfide, disulfur complex, nanocrystalline, oxidation*

INTRODUCTION

Molybdenum sulfide has recently emerged as a promising catalyst for the hydrogen evolution reaction (HER) in water that bears significant implications for the ongoing energy and environmental challenges.[1−8] In comparison with Pt group metals, which have been the most widely used HER catalysts to date but are too precious to be useful for mass production of hydrogen, molybdenum sulfide is earth-abundant and can be manufactured in cost-effective ways. However, the catalytic performance, including Tafel slope, turnover frequency (TOF), and stability, of molybdenum sulfide is much worse than that observed for Pt. Therefore, the key issue to make molybdenum sulfide a HER catalyst useful for practical applications is to substantially improve its catalytic performance.

The development of high-performance molybdenum sulfide HER catalysts has generally been delayed by a limited fundamental understanding of the correlation between the catalytic performance and the physical (compositional and structural) features of molybdenum sulfide materials. Despite a considerable number of studies on the catalysis of molybdenum sulfide with various physical features,[1,7−10] the results usually vary in a broad range and sometime even conflict with each other. It is thus difficult to compare these results and draw decisive conclusions on the catalysis−physical features

Received: October 23, 2014
Revised: November 26, 2014
Published: December 4, 2014

correlation. For examples, numerous studies have demonstrated low Tafel slopes of around 40 mV/dec for various molybdenum sulfide materials, such as molybdenum disulfide (MoS_2) mixed with graphene or carbon nanotubes,[11−14] molybdenum trisulfide (MoS_3),[3,13,15−17] $Mo_3S_{13}^{2-}$ clusters,[18] and chemically processed MoS_2 nanosheets.[4,6] This Tafel slope is very close to that observed for Pt (30 mV/dec) and stands as the lowest ever reported for all kinds of non-precious-metal HER catalysts.[19−21] However, the mechanism underlying the low Tafel slope has remained controversial, which has hindered a further improvement of the catalytic performance. Some claim that MoS_3 only serves as a precatalyst and can be reduced to the true catalyst MoS_x,[3,17,22] while others argue that the low Tafel slope is due to the presence of edge sites S_2^{2-} or the coupling between the catalyst and its support such as graphene or carbon nanotubes.[11−13,15,18] Additionally, despite the low Tafel slopes, these molybdenum sulfide materials usually show low stability with obvious decrease in catalytic activities after tens or hundreds of cycles. It is not clear what causes the instability and how the stability could be correlated to the physical feature of the materials, which essentially prevents any effective efforts to improve the stability.

Much of the ambiguity of the results in references is rooted in the limited capability of the existing synthetic approaches for molybdenum sulfide to precisely control the composition and crystalline structure of the resulting materials. Current approaches to prepare the molybdenum sulfide materials with low Tafel slopes are all wet chemical based, including hydrothermal or thermal decomposition or electrochemical processing.[3,4,11−13,15−18,22] These approaches can only offer limited controllability and fragile reproducibility. For instance, the materials made using similar hydrothermal or thermal decomposition processes may show substantial variation in catalytic performance, though the compositions might seem to be similar.[12,15,16] Even minor changes in the experimental conditions, such as temperature or electrochemical potential, could result in dramatic changes in the catalytic performance and composition of the resulting materials.[3,15,22] Additionally, the catalytic performance often shows a dependence on parameters other than the intrinsic compositional and structural features of the catalyst, such as the type of supporting substrate, the loading of the catalyst, and the involvement of activation processes.[3,12,13,15,17] All these factors make it very difficult to establish an unambiguous correlation between the catalytic performance and the compositional and structural features of molybdenum sulfide.

Here we unambiguously elucidate the dependence of the catalytic performance of molybdenum sulfide, including Tafel slope, TOF, and stability, on its composition and crystallinity. Our success is built upon a new ambient-pressure chemical vapor deposition (AP-CVD) process that we have developed to synthesize molybdenum sulfide materials with precisely controlled physical features. This unique synthetic capability has allowed us to systematically investigate the catalytic performance as functions of the composition and crystalline structures. Our studies indicate that the crystallinity of molybdenum sulfide plays an overwhelmingly important role in the catalytic performance. It can affect the three figures of merit (Tafel slope, TOF, and stability) of catalytic performance in opposite directions. Generally, a molybdenum sulfide with low crystalline quality exhibits lower Tafel slopes, while highly crystalline materials show higher TOFs and better stability. Our studies also indicate that the composition is not that important. The materials with low crystalline quality always show similar Tafel slopes and TOFs regardless of the S:Mo stoichiometric ratio, which varies in the range of 2−3. The result may provide very useful guidance for the rational design of molybdenum sulfide HER catalysts with optimal catalytic performance. It indicates that the key is to engineer the crystalline structure so as to balance the contradictory effects of crystallinity on the different aspects of the catalytic reaction.

More specifically, the low crystalline quality molybdenum sulfide materials that we grew at low temperatures (≤420 °C) are able to provide a low Tafel slope of 40 mV/dec, regardless of the S:Mo stoichiometric ratio. These include amorphous MoS_3, amorphous MoS_2, and few-layer nanocrystalline MoS_2 with a lateral size of 5−30 nm. In contrast, the highly crystalline (polycrystalline and single crystalline) MoS_2 grown at higher temperatures (≥500 °C) shows Tafel slopes of 80−90 mV/dec or higher. Our DFT calculations suggest that the terminal disulfur complexes S_2^{2-}, which may exist in MoS_3 and also likely at the edge of low crystalline quality MoS_2 due to its structural disorder, could be the true catatically active sites responsible for the low Tafel slope. Although it provides a worse Tafel slope, the highly crystalline MoS_2 can give rise to TOFs 2 orders of magnitude higher than the low crystalline quality molybdenum sulfide. Additionally, the materials with higher crystalline quality generally show better stability. Nanocrystalline MoS_2 is more stable than amorphous MoS_3 and MoS_2, and the stability of highly crystalline MoS_2 is even better. We find that the catalytic instability is related to the oxidation of the catalyst by ambient oxygen and that the molybdenum sulfide materials with higher crystalline quality may better resist the oxidation. Our result clearly indicates that the few-layer nanocrystalline MoS_2 with a lateral size of 5−30 nm provides a more promising platform than amorphous and highly crystalline molybdenum sulfide for the development of high-performance, low-cost HER catalysts due to its combination of low Tafel slopes and good stability. To further illustrate this notion, we developed a molybdenum sulfide catalyst by careful engineering of the crystallinity that shows a Tafel slope of 40 mV/dec, an exchange current density of 3.5 $\mu A/cm^2$, and remarkable stability with the cathodic current remaining constant over >10000 cycles. We believe that the performance of this catalyst could be further improved by improving the relatively low exchange current density through use of rougher substrates (increasing surface areas) or doping (increasing electrical conductivity).

EXPERIMENTAL METHODS

Synthesis of Molybdenum Sulfide Materials. The molybdenum sulfide materials were synthesized in a tube furnace via an ambient-pressure chemical vapor deposition process. In a typical growth, 0.04 g of molybdenum chloride ($MoCl_5$) powder (99.99%, Sigma-Aldrich) and 0.2 g of sulfur powder (Sigma-Aldrich) were placed at the upstream of the furnace. Receiving substrates were placed in the downstream of the tube. Typical conditions for the synthesis include an Ar flow rate of 50 sccm and a growth temperature varying between 200 and 600 °C. During the synthesis, the vapor of the precursor materials reacted to produce gaseous molybdenum sulfide species, which could subsequently precipitate onto the receiving substrates. The loading of the resulting materials was controlled by changing the amount of precursor. Most of the materials studied in this work were grown on graphite substrates, but the materials used for cross-sectional SEM and XRD character-

dx.doi.org/10.1021/cs501635v | ACS Catal. 2015, 5, 448−455

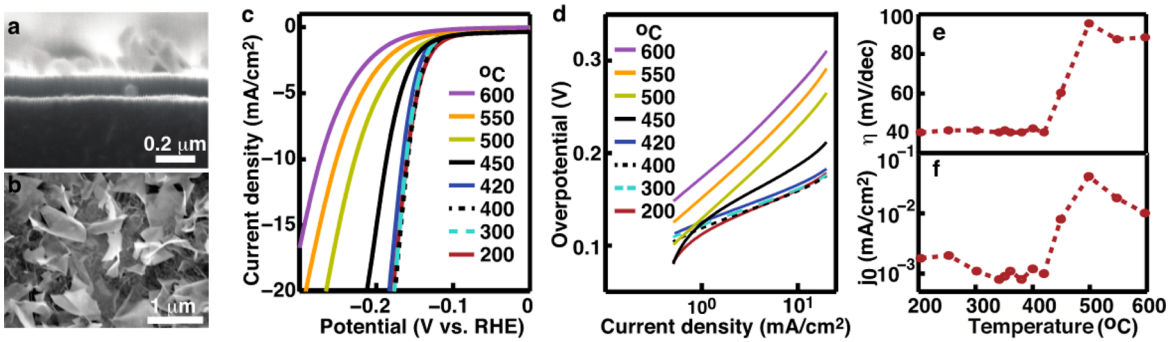

Figure 1. Catalytic activities of molybdenum sulfide materials grown at different temperatures. (a) SEM image of the materials grown at 300 °C. A sideview image is given here to illustrate the thickness of the film. (b) SEM image of the materials grown at 600 °C. (c) Polarization curves and (d) Tafel plots of the molybdenum sulfide materials grown at different temperatures. The growth temperatures are labeled as shown. (e) Tafel slopes and (f) exchange current densities of the molybdenum sulfide materials as a function of the growth temperature.

izations were grown on glassy carbon substrates. Glassy carbon can provide better illustration for the distinction between the substrate and the deposited film in cross-sectional SEM images, which is very difficult when using rough graphite substrates. Glassy carbon also provides a better substrate for the XRD measurements because of the lower background signal due to its lower crystalline quality. We have confirmed that the use of two different substrates does not affect the conclusion of this work at all. These two substrates may enable different surface areas in the catalysts owing to different surface roughness, but the catalysts grown on the two different substrates show essentially identical Tafel slopes and TOFs.

Material Characterization. The structure and composition of the synthesized materials were characterized by tools including scanning electron microscopy (SEM, JEOL JSM-6400F), transmission electron microscopy (TEM, JEOL-2010F), Raman spectroscopy (Renishaw-1000) with an excitation wavelength of 514.5 nm, X-ray diffraction (XRD, Rigaku SmartLab X-ray diffractometer using Cu Kα radiation), and X-ray photoelectron spectroscopy (XPS, SPECS System with PHOIBOS 150 analyzer using an Mg Kα X-ray source). During the XPS measurement, a commercial MoS_2 sample (SPI) was always placed along with the synthesized materials and the Mo $3d_{5/2}$ peak (229.5 eV) of the commercial MoS_2 was used for calibration. The XPSPEAK software version 4.1 was used for fitting, and the spectral peaks were fitted using a mixed Gaussian−Lorentzian line shape and Shirley baselines.

Electrochemical Characterization. The electrochemical characterization was performed in 0.5 M H_2SO_4 using a CH Instrument electrochemical analyzer (Model CHI604D), a saturated calomel reference electrode (SCE), and as-grown molybdenum sulfide on substrates as the working electrode. We used both graphite plates and coiled Pt wires as the counter electrodes in experiments and found that using either of the counter electrodes gave rise to essentially identical results. Nitrogen gas was bubbled into the electrolyte throughout the experiment. While all the electrochemical characterization studies were performed using a saturated calomel reference electrode (SCE), the potential values mentioned in the electrochemical study are referenced to a reversible hydrogen electrode (RHE). Calibration of the reference electrode for the reversible hydrogen potential was performed using a platinum (Pt) disk as working electrode and a coiled Pt wire as counter electrode in 0.5 M H_2SO_4. The electrolyte was purged with ultrahigh-purity hydrogen (Airgas) during the calibration. The potential shift of the SCE was found to be −0.262 V vs RHE. The electrocatalysis was measured using linear sweeping from +0 to −0.3 V (vs RHE) with a scan rate of 5 mV/s. The electrolyte resistance and capacitance of the electrocatalysts were characterized using electrochemical impedance spectroscopy (EIS) under a potential of −0.15 V (vs RHE). The ac impedance was measured within the frequency range of 10^6−1 Hz with a perturbation voltage amplitude of 5 mV. An equivalent Randles circuit model was fit to the data with ZSimpWin software to determine the system resistance and capacitance (see the EIS results in Figure S1 in the Supporting Information). The stability of the electrocatalyst was examined by continuously cycling the potential between +0.2 and −0.3 V at a scan rate of 50 mV/s. The lower voltage limit was chosen to drive a current density of approximately 30 mA/cm^2.

RESULTS AND DISCUSSION

The ambient-pressure CVD process is similar to what we previously developed for the synthesis of MoS_2 atomic-scale films except for the pressure and temperature.[23] Briefly, $MoCl_5$ and sulfur were used as precursor materials and placed at the upstream of a tube furnace flown with Ar gas. The precursors may sublimate and react in the vapor phase at elevated temperatures to yield molybdenum sulfide species, which can subsequently precipitate on receiving substrates located at the downstream of the furnace. This CVD process allows us to precisely control the composition, crystalline structure, and loading of the resulting materials by controlling experimental conditions such as growth temperature. Generally, a low growth temperature (≤420 °C) may result in the formation of thin films, whose thickness is typically controlled to be ∼100 nm (Figure 1a), while a high temperature (≥500 °C) can give rise to flowerlike nanosheets, each of which has a thickness of tens of nanometers and a lateral size of micrometers (Figure 1b).

The catalytic activity of the synthesized materials strongly depends on the growth temperature. Figure 1c,d shows the polarization curves and corresponding Tafel plots, which are all *iR* corrected, of the materials grown at temperatures ranging from 200 to 600 °C (more results can be seen in Figure S2 in the Supporting Information). Very interestingly, the catalytic performance remains to be similar for all the materials grown at low temperatures (≤420 °C) but tends to monotonically decrease with an increase in the growth temperature when the growth temperature is beyond 420 °C. This temperature-dependent catalytic activity can be better understood from the perspectives of Tafel slope and exchange current density. We can obtain the Tafel slope and exchange current density by

dx.doi.org/10.1021/cs501635v | ACS Catal. 2015, 5, 448−455

fitting the Tafel plots (Figure 1d and more results in Figure S2b in the Supporting Information) to the equation of $\eta = \rho \log j + \log j_0$, where η is the overpotential (vs RHE), j the current density, j_0 the exchange current density, and ρ the Tafel slope.[24] We can find that both the Tafel slope and exchange current density of the materials show a step function like dependence on the growth temperature (Figure 1e,f). For the materials grown at low temperatures (≤420 °C), the Tafel slope and exchange current density are approximately constant at 40 mV/dec and ~1.0×10^{-6} A/cm^2, respectively. However, the values dramatically jump to 80−90 mV/dec and 10−30 × 10^{-6} A/cm^2 for the materials grown at high temperatures (≥500 °C). The growth temperature in between (420−500 °C) makes a transition zone. For instance, the materials grown at 450 °C may show a Tafel slope of 50−60 mV/dec and an exchange current density in the range of (2−8) × 10^{-6} A/cm^2. Note that the Tafel slope of the materials grown at high temperatures (≥500 °C) decreases with cyclic voltammetry, and the value of 80−90 mV/dec is the stable result after numerous cycles (Figure S3 in the Supporting Information). For the convenience of discussion, if not specified, we refer to temperatures ≤420 °C as low temperatures, ≥500 °C as high temperatures, and those in between as intermediate temperatures in the following text.

We can exclude any possible effects from the underlying substrate because the deposited films are thick enough (~100 nm typically) to prevent the influence of the substrate on the catalytic reaction. We can also exclude the possible difference in loading of the catalysts to be the reason for the observed temperature-dependent Tafel slopes and exchange current densities, although other researchers reported that the difference in catalyst loading could give rise to different Tafel slopes.[17] This is first because the loading in all the catalyts studied in Figure 1 (and Figure S2 in the Supporting Information) were controlled to be comparable in the range of 300−500 μg/cm^2. Additionally, we found in experiments that, while the loading of our catalysts does not affect the Tafel slope, although it may substantially affect the exchange current density (Figure S4 in the Supporting Information). Instead, our experimental results suggest that the temperature-dependent catalytic activity is rooted in the different compositions and crystallinities of the materials grown at different temperatures.

The composition of the materials depends on the growth temperature, gradually changing from MoS_3 to MoS_2 with an increase in the growth temperature. Figure 2a shows the XPS collected from the materials grown at different temperatures. Also given are the corresponding peak fittings. We can find an obvious temperature dependence in the S 2p spectra but not the Mo 3d spectra. Regardless of the growth temperature, the Mo 3d spectra always show a doublet with similar binding energies at 229.50 eV ($3d_{5/2}$) and 232.65 eV ($3d_{3/2}$). This indicates that the Mo mainly maintains a 4+ oxidation state as Mo^{4+} in all the materials. In contrast, the S 2p spectra show substantial temperature dependence. For the materials grown at low temperatures (≤420 °C), two doublets ($2p_{3/2}$ and $2p_{1/2}$) can be found in the S 2p spectra, one at energies of 162.2 and 163.4 eV that may be attributed to the terminal S_2^{2-} in MoS_3 and/or the S^{2-} in MoS_2 (yellow curves) and the other at higher energies (cyan curves) that can be assigned to the bridging S_2^{2-} and apical S^{2-} in MoS_3.[25] Note that a third doublet at even higher energies (brown curves) resulting from residual sulfur element S^0 can be found at the materials grown at the lowest temperatures (200 °C), but it is not of interest to us because S^0

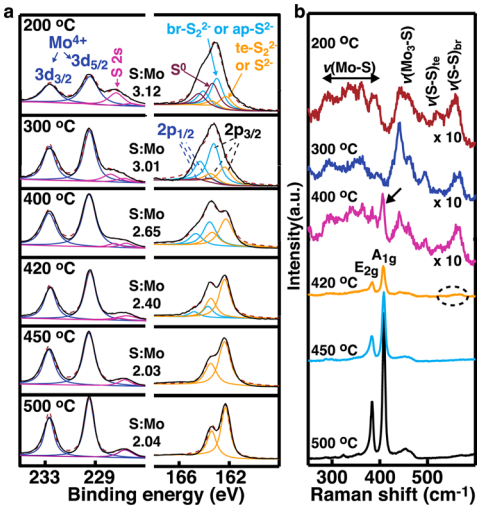

Figure 2. Dependence of the compositions of molybdenum sulfide on the growth temperature. (a) XPS spectra and corresponding peak fitting of the molybdenum sulfide materials grown at different temperatures. The growth temperature and the assignment of fitted peaks are given as shown. Also given is the S:Mo ratio estimated from quantitative analysis of the XPS measurements. (b) Raman spectra of the molybdenum sulfide materials grown at different temperatures. The growth temperature and assignment of the Raman peaks are given in the figure. For visual convenience, the intensities of the Raman spectra of the materials grown at 400 °C of lower temperatures are multiplied by a constant of 10. The arrow indicates the Raman peak of crystalline MoS_2 in the materials grown at 400 °C, and the dashed circle is to indicate the Raman peaks of MoS_3 in the materials grown at 420 °C (see also Figure S5 in the Supporting Information).

is not catalytically active and the existence of the S^0 does not seem to affect the catalytic performance, as evidenced by the similar catalytic performances in materials both with S^0 and without S^0 (Figure 1). Only one doublet ($2p_{3/2}$ and $2p_{1/2}$) at the energy of 162.2 and 163.4 eV can be found with the materials grown at temperatures ≥450 °C. Quantitative analysis of the XPS results demonstrates that the S:Mo stoichiometric ratio (elemental sulfur is not counted) in the materials gradually decreases from ~3 to ~2 with an increase in the temperature. These results indicate that the composition of the synthesized materials evolves from MoS_3 to MoS_2 with the growth temperature. More specifically, the material synthesized at temperatures lower than 400 °C consists of MoS_3, mainly MoS_2 at a growth temperature ≥450 °C, and a mixture of MoS_3 and MoS_2 at growth temperatures of 400 and 420 °C. We can further estimate the MoS_3:MoS_2 molar ratios to be 7:3 and 4:6 in the materials grown at 400 and 420 °C, respectively. This temperature-dependent composition has been confirmed by Raman measurements (Figure 2b). The materials grown at temperatures lower than 400 °C show Raman features similar to those previously reported for MoS_3 and $[Mo_3S_{13}]$,[2−18,25−27] while those grown at the temperatures ≥450 °C only show the characteristic peaks of MoS_2, A_{1g} and E^1_{2g}.[28] The Raman features of both MoS_3 and MoS_2 can be found in the materials grown at 400 and 420 °C.

The crystalline structure of the synthesized materials is also dependent on the growth temperature, evolving from amorphous to single crystalline with an increase in the temperature. Figure 3 shows the TEM images and electron diffraction patterns collected from the materials synthesized at different temperatures. The materials were transferred from the

dx.doi.org/10.1021/cs501635v | ACS Catal. 2015, 5, 448−455

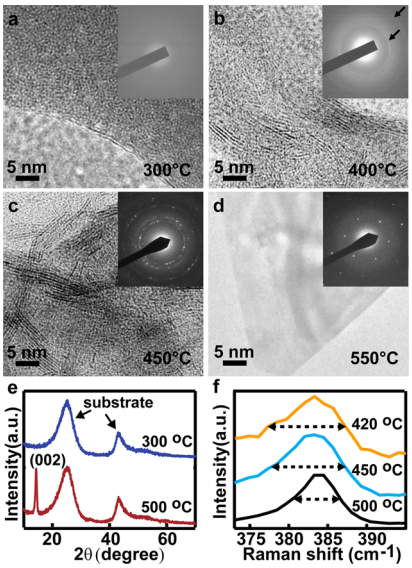

Figure 3. Dependence of the crystallinity of molybdenum sulfide on the growth temperature. TEM images and electron diffraction patterns of the molybdenum sulfide materials grown at (a) 300 °C, (b) 400 °C, (c) 450 °C, and (d) 500 °C. The arrow in the inset of (b) points toward weak diffraction rings. A larger version of this diffraction pattern is given in Figure S6 in the Supporting Information. (e) XRD results collected from the typical molybdenum sulfide materials grown at low temperatures (300 °C) and high temperatures (500 °C). (f) E^1_{2g} Raman peak of the MoS_2 grown at temperatures of 420, 450, and 500 °C, which is extracted from Figure 2b. The dashed line indicates the full width at half-maximum (fwhm) of the peak.

original growth substrates (graphite) to TEM grids by simply scratching for the characterization. The materials grown at very low temperatures such as 300 °C are amorphous with no crystalline pattern in the electron diffraction result and no characteristic layered structures in the TEM image (Figure 3a). In contrast, few-layer nanocrystalline MoS_2 with a lateral size of 5−30 nm can be found in the materials grown at 400 and 420 °C, and the weak rings in the corresponding electron diffraction results indicate that the crystallinity of these materials is low (Figure 3b and Figure S7 in the Supporting Information). The materials grown at higher temperatures show apparently higher crystallinity, appearing to be polycrystalline films at a growth temperature of 450 °C and single-crystalline nanosheets with a lateral size of micrometers at temperatures of 500 °C or higher (Figure 3c,d). It is difficult to precisely identify the grain size in the polycrystalline film grown at 450 °C, but we can roughly estimate that it should be in the range of tens to hundreds of nanometers. XRD and Raman measurements can further confirm the increase of crystallinity with the growth temperature. For instance, the XRD result of the materials grown at 300 °C shows no obvious diffraction peaks, but those of the materials grown at 500 °C show well-defined peaks corresponding to the diffraction from the (002) planes of MoS_2 (Figure 3e). Additionally, the Raman scattering from the materials grown at low temperatures (≤420 °C) is very weak but its intensity monotonically increases by up to more than 1 order of magnitude at higher growth temperatures (Figure 2b). This indicates an increase in crystallinity, since the volume (loading) of materials is controlled to be comparable in experiments. We can also find that the full width at half-maximum of the E^1_{2g} peak, which is widely used as an indicator for the crystalline quality of MoS_2,[28] decreases with an increase in the growth temperature (Figure 3f). This provides further support for the increase of crystallinity with the growth temperature.

We can obtain useful insight by comparing the temperature-dependent Tafel slopes and exchange current densities with the composition and crystallinity of the synthesized materials, as shown in Table 1. We found in experiments that the exchange current density of a given materials is linearly proportional to the surface area of the materials (Figure S8 in the Supporting Information). Therefore, in order to compare the intrinsic catalytic activities of different materials, we derive the TOFs, which represent the catalytic activity of each surface atom, for these materials by normalizing the exchange current density with respect to the number of MoS_2 atoms at the surface. The surface area of the synthesized materials is estimated from the ratio of the measured capacitance with respect to the double-layer capacitance of atomically smooth MoS_2 materials (66.7 $\mu F/cm^2$) that we measured previously.[29] By comparing the results, we can find that the composition does not matter much for the catalytic performance. The materials grown at low temperatures (≤420 °C) all show similar Tafel slopes and TOFs, regardless of the specific S:Mo stoichiometric ratio, which varies from 3 to 2. The comparison also indicates that the crystallinity plays an overwhelmingly important role and can impact the Tafel slope and TOF in different directions. Generally, the materials with low crystallinity, including amorphous MoS_3, amorphous MoS_2, and few-layer nanocrystalline MoS_2 with a lateral size of 5−30 nm, show low Tafel slopes (~40 mV/dec) and low TOFs ($(1-3 \times 10^{-5}$ s^{-1}), while the highly crystalline MoS_2 shows high Tafel slopes of 80−90 mV/dec or higher and high TOFs of $(3-5) \times 10^{-3}$ s^{-1}. The distinct Tafel slopes indicates different rate-determining steps for the HER at the molybdenum sulfide materials with low and high crystallinity. Our DFT calculations suggest that the terminal disulfur complex S_2^{2-} could be the true catalytically active site responsible for the low Tafel slope. Terminal S_2^{2-} exists in MoS_3 and likely also at the edges of low crystalline quality MoS_2 due to its structural disorder. The DFT calculations indicate that terminal S_2^{2-} can provide the lowest adsorption free energy for hydrogen atoms. As a result of the low energy barrier for H_2 formation, the rate-limiting step at terminal S_2^{2-} may likely be electron transfer processes, which may result in a Tafel slope of 40 mV/dec (see Density Functional Theory

Table 1. Comparison of the Catalytic Activities and Compositional/Structural Features of Molybdenum Sulfide Materials

temp (°C)	composition	structure	Tafel slope (mV/dec)	J_0 ($\mu A/cm^2$)	capacitance (mF/cm^2)	TOF (10^{-3} s^{-1})
200−380	MoS_3	amorphous	39	~1−2	10−20	0.01−0.03
400	MoS_3 (70%), MoS_2 (30%)	amorphous nanocrystalline	42	1.2	10	0.027
420	MoS_3 (40%), MoS_2 (60%)	amorphous nanocrystalline	40	1.0	12	0.012
450	MoS_2	polycrystalline	50−60	8	8	0.14
500−600	MoS_2	single crystalline	80−90	10−40	0.5−1.5	2.5−3.5

dx.doi.org/10.1021/cs501635v | ACS Catal. 2015, 5, 448−455

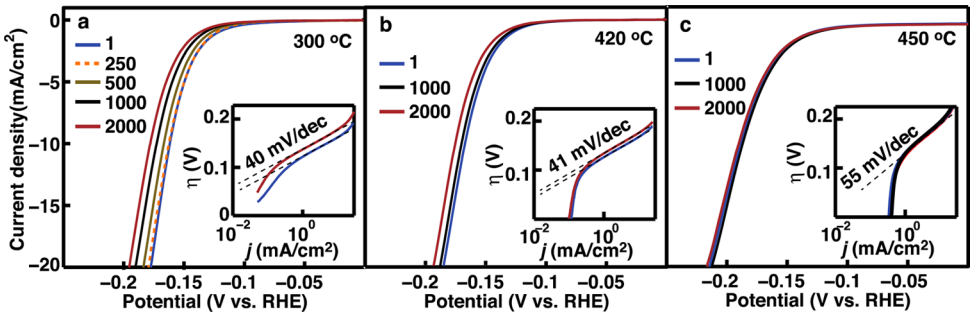

Figure 4. Dependence of the catalytic stability of molybdenum sulfide on the growth temperature. Polarization curves of the molybdenum sulfide materials grown at (a) 300 °C, (b) 420 °C, and (c) 450 °C with different cycles. The insets give corresponding Tafel plots in which only the results for the 1st and 2000th cycle are given for visual convenience.

Calculations in the Supporting Information). Additionally, the remarkable difference in TOF values between the materials with low and high crystallinity could be due to the different dynamics of these rate-determining steps. Another possible reason might be the different electrical conductivities of the materials. Many recent studies, including our previous work, have demonstrated that higher electrical conductivities can enable higher exchange current densities.[4,5,29]

The stability of the synthesized materials shows dependence on the crystallinity as well, generally increasing with the degree of crystallinity. Of our particular interest is the stability of the materials grown at low temperatures (≤420 °C), which can provide attractive low Tafel slopes. We tested the stability by performing cyclic voltammetry (CV) in the potential range from +0.2 to −0.3 V (vs RHE) and monitored changes in the cathodic current during the cycling process. Without losing generality, Figure 4 shows the results obtained from typical materials grown at 300 and 420 °C. The result of the materials grown at even higher temperatures such as 450 °C is also given as a reference. The materials grown at 300 °C, which mainly consists of amorphous MoS_3, can be found showing a monotonic decrease in cathodic current with the cycling after ∼250 cycles (Figure 4a). In contrast, the material grown at 420 °C that involves a substantial amount of nanocrystalline MoS_2 may maintain unchanged current for up to ∼1000 cycles (Figure 4b). The materials grown at 450 °C or higher temperatures, which are of higher crystalline quality, are even more stable by showing constant currents for thousands of cycles (Figure 4c and also see Figure S9 in the Supporting Information).

The observed instability in the catalytic activity can be more specifically ascribed to the lose of catalytically active sites. From the Tafel plots given in the insets to Figure 4a,b, we can find that the Tafel slope stays constant while the exchange current density decreases during the cycling process. Additionally, in experiments we observed a decrease in the capacitance of the catalysts during the cycling that is reasonably proportional to the decrease of the exchange current density (Figure S10 in the Supporting Information). This suggests that the TOF (the catalytic activity at each site) is essentially unchanged during the cycling. Given the unchanged Tafel slope and TOF, it is reasonable to conclude that the instability in the catatylic activities is caused by the decrease in the number of catalytically active sites.

To better understand the stability, we monitored the composition and crystalline structure of the catalyst by performing numerous ex situ XPS and Raman measurements during the CV process. The XPS results indicate obvious compositional changes in the low crystalline quality materials (grown at temperatures ≤420 °C) during the cycling: generally the lower the crystallinity, the more change in the composition (Figure 5a,b). However, no obvious compositional change can

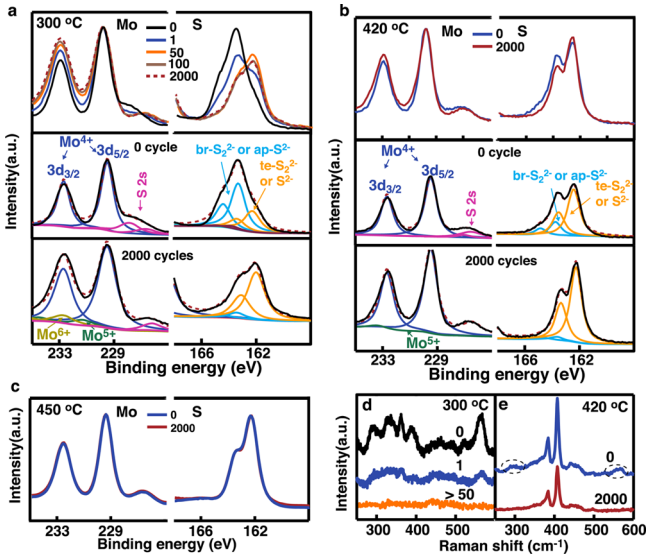

Figure 5. Dependence of the compositional stability of molybdenum sulfide on the growth temperature. XPS spectra collected from the molybdenum sulfide materials grown at (a) 300 °C, (b) 420 °C, and (c) 450 °C that are subject to different scanning cycles during the continuous CV process. The number of cycles for each result is labeled as shown. For the materials grown at 300 and 420 °C, the peak fitting for the results collected before the cycling and after 2000 cycles are also given with the assignment of fitted peaks given in the figure. Also given are the Raman spectra collected from the molybdenum sulfide materials grown at (d) 300 °C and (e) 420 °C after being subject to different cycles, in which the number of cycles for each result is labeled. The dashed circles in (e) indicate the characteristic Raman peaks of MoS_3, which disappear after the cycling.

be seen in the materials grown at the temperatures ≥450 °C, which is highly crystalline (Figure 5c). The XPS results indicate two compositional changes in the low crystalline materials. One is the reduction of MoS_3 to MoS_2, which is evidenced by the S 2p spectra. The intensity of the doublet in the S 2p spectra that corresponds to the bridging S_2^{2-} and/or apical S^{2-} shows obvious decrease with the cycling (cyan curves in Figure 5a,b). For example, the S 2p spectrum of the materials grown at 300 °C (mainly consisting of MoS_3) is very similar to that of MoS_2 after tens of cycles (Figure 5a). This suggests the conversion of

dx.doi.org/10.1021/cs501635v | ACS Catal. 2015, 5, 448−455

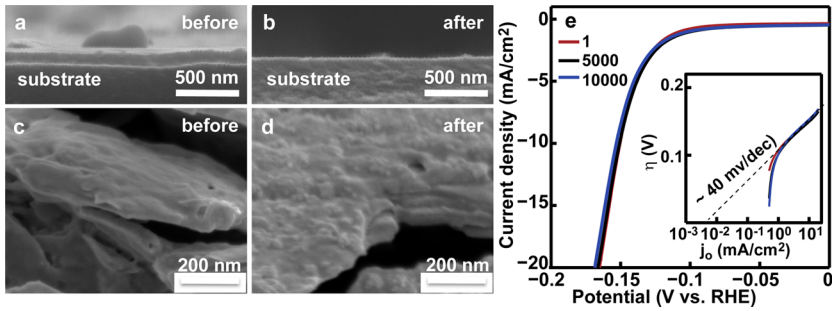

Figure 6. Improvement in the stability of molybdenum sulfide materials by crystallinity engineering. Cross-sectional SEM images of the molybdenum sulfide films grown at (a) 300 °C and (b) 400 °C before the cycling (before) and after 2000 cycles (after). The thickness of the molybdenum sulfide films is indicated by arrows. (c) Polarization curves and corresponding Tafel plots of the molybdenum sulfide materials grown at 400 °C followed by a mild annealing in the presence of sulfur at the same temperature as for the growth.

MoS_3 to MoS_2, which is due to the reduction of MoS_3 at negative potentials. Raman measurements confirm the conversion, as the characteristic Raman peaks of MoS_3 disappear after tens of cycles (Figure 5d,e). The Raman spectra of the materials grown at 300 °C are featureless after the conversion, suggesting that the resulting MoS_2 is amorphous. Other researchers also reported a similar reduction of MoS_3 to MoS_2 at negative potentials.[3,17,22] The other change in the composition is the oxidation of MoS_2, as indicated by the Mo 3d spectra. The intensity of the peak at the higher binding energy in the Mo 3d spectra can be seen increasing with the cycling; again, the change is more obvious in the materials with lower crystallinity. Peak fitting analysis indicates that this is due to the appearance of higher oxidation states of Mo (Mo^{6+} and Mo^{5+}), which results from the oxidation of Mo^{4+}. The oxidation is likely caused by the oxygen in an ambient environment instead of the applied electrochemical potential, as the electrochemical potential is too low (<+0.2 V vs RHE) to oxidize molybdenum sulfide. Our experiments were performed in an ambient environment, and the electrochemical cell used in experiments was not perfectly sealed. Although N_2 was purged during the experimental process, the imperfect setup could allow a trace amount of oxygen to get into the system to oxidize the catalyst materials. The molybdenum sulfide with higher crystalline quality may better resist the oxidation and thus exhibit better stabilities.

The experimental results also suggest that the observed catalytic instability is not due to the MoS_3/MoS_2 conversion but is related to the oxidation of molybdenum sulfide materials. From the XPS and Raman measurements, we find that the reduction of MoS_3 to MoS_2 can be finished in ~50 cycles (Figure 5a,d). However, the catalytic performance of the materials may maintain unchanged for more cycles: for instance, 250 and 1000 cycles at the materials grown at 300 and 400 °C, respectively (Figure 5a,b). The extension of constant cathodic currents beyond the MoS_3/MoS_2 conversion clearly indicates that the conversion process does not affect the catalytic activity. This result also indicates that the bridging S_2^{2-} and/or apical S^{2-} are not the major catalytically active sites, which provides additional evidence for our hypothesis that terminal S_2^{2-} is the true catalytically active site responsible for the low Tafel slope. In contrast, the oxidation that converts molybdenum sulfide to molybdenum oxide such as MoO_3 can effectively decrease the number of catalytically active sites, because molybdenum oxide is not catalytically active for the hydrogen evolution reaction. This may lead to a decrease in the exchange current density, as we observed. Other researchers also recently demonstrated that the oxidation of molybdenum sulfide materials could cause a substantial decrease in the catalytic activity.[30,31] As further evidence for the oxidation and its effect on the catalytic activities, we observed a substantial loss of the catalyst materials during the catalytic reaction. This is evidenced by a decrease in the thickness of the synthesized film (Figure 6a,b). A decrease in the thickness is more obvious in the materials with lower crystallinity, which is consistent with the XPS measurements that indicate more oxidation in the materials with lower crystallinity. Molybdenum oxide such as MoO_3 is weakly soluble in water and may be partially dissolved in the electrolyte solution. The continuous oxidation and dissolution of the oxide may eventually lead to significant loss of the catalyst materials.

CONCLUSION

In conclusion, we have unambiguously correlated the catalytic performance, including Tafel slope, TOF, and stability, to the composition and crystallinity of molybdenum sulfide materials by leveraging on a new CVD process that we have developed to synthesize molybdenum sulfide materials with controlled physical features. We demonstrate that the crystallinity plays a critical role in determining the catalytic performance, while the composition does not matter much. The crystallinity can strongly impact the three figures of merit (Tafel slope, TOF, and stability) of the catalytic performance in opposite directions. Generally, the materials with low crystallinity may provide low Tafel slopes (~40 mV/dec), while highly crystalline molybdenum sulfide shows higher TOFs (by 2 orders of magnitude) and better stabilities. On the other hand, molybdenum sulfide materials with low crystallinity all show similar Tafel slopes and TOFs, regardless of the S:Mo stoichiometric ratio varying in the range of 2−3. These include amorphous MoS_3, amorphous MoS_2, and few-layer nanocrystalline MoS_2 with a lateral size of 5−30 nm. Our DFT calculations suggest that the terminal disulfur complex S_2^{2-} could be the true catalytically active site responsible for the low Tafel slope. Terminal S_2^{2-} may exist in MoS_3 and also likely at the edge of low crystalline quality MoS_2 due to its structural disorder. We also find that the catalytic instability is related to the oxidation of molybdenum sulfide materials by ambient oxygen, and the materials with higher crystallinity may provide better resistance to the oxidation.

This work represents a significant advance with respect to the previous understanding of the catalysis of molybdenum sulfide, which usually just simply states that edge sites are the catalytically active sites but does not specify how the edge

dx.doi.org/10.1021/cs501635v | ACS Catal. 2015, 5, 448−455

sites could affect the Tafel slope, exchange current density, and stability. Our result can provide useful guidance for the rational design of molybdenum sulfide HER catalysts with optimal catalytic performance, including low Tafel slopes, high exchange current densities, and high stability. It indicates that the key issue is to carefully control the crystalline structure for the purpose of balancing the contradictory effects of crystallinity on the different aspects of the catalytic performance. Our result also explicitly points out that nanocrystalline MoS_2 with few-layer nanoclusters in a lateral size of 5−30 nm may provide a more promising platform than either amorphous or highly crystalline molybdenum sulfide, due to its combination of low Tafel slopes and good stability. To illustrate this notion, we developed a MoS_2 catalyst by engineering the crystallinity that shows a Tafel slope of 40 mV/dec, an exchange current density 3.5 $\mu A/cm^2$, and remarkable stability, with the cathodic current remaining constant over >10000 cycles (Figure 6c), which is among the best values ever reported. This improvement in stability with no compromise in Tafel slope is achieved by a mild annealing of the nanocrystalline MoS_2 grown at 400 °C in the presence of sulfur and under the same temperature as the growth. To further improve the catalytic performance would require a substantial increase in the relatively low exchange current density. We believe that this can be achieved by using rougher substrates to increase surface areas or by doping to improve the electrical conductivity.

■ ASSOCIATED CONTENT

Supporting Information

The following file is available free of charge on the ACS Publications website at DOI: 10.1021/cs501635v.

More experimental results on the compositional, structural, and electrochemical characterizations of the synthesized molybdenum sulfide materials, as well as density functional theory calculation results (PDF)

■ AUTHOR INFORMATION

Corresponding Authors

*E-mail for Y.L.: yanpengli@hit.edu.cn.

*E-mail for L.C.: lcao2@ncsu.edu.

Author Contributions

⊥Y.P. and Y.Y. contributed equally.

Notes

The authors declare no competing financial interest.

■ ACKNOWLEDGMENTS

This work was supported as part of the Center for the Computational Design of Functional Layered Materials, an Energy Frontier Research Center funded by the U.S. Department of Energy, Office of Science, Basic Energy Sciences, under Award # DE-SC0012575. The authors acknowledge useful discussions with S. Y. Huang and the use of the Analytical Instrumentation Facility (AIF) at North Carolina State University, which is supported by the State of North Carolina and the National Science Foundation. The computational studies by Y.H., R.A.N., and W.A.G. were supported by the Joint Center for Artificial Photosynthesis, a DOE Energy Innovation Hub, supported through the Office of Science of the U.S. Department of Energy under Award Number DE-SC0004993.

■ REFERENCES

(1) Laursen, A. B.; Kegnaes, S.; Dahl, S.; Chorkendorff, I. *Energy Environ. Sci.* **2012**, *5*, 5577.

(2) Jaramillo, T. F.; Jorgensen, K. P.; Bonde, J.; Nielsen, J. H.; Horch, S.; Chorkendorff, I. *Science* **2007**, *317*, 100.

(3) Merki, D.; Fierro, S.; Vrubel, H.; Hu, X. L. *Chem. Sci.* **2011**, *2*, 1262.

(4) Lukowski, M. A.; Daniel, A. S.; Meng, F.; Forticaux, A.; Li, L.; Jin, S. *J. Am. Chem. Soc.* **2013**, *135*, 10274.

(5) Voiry, D.; Yamaguchi, H.; Li, J.; Silva, R.; Alves, D. C. B.; Fujita, T.; Chen, M.; Asefa, T.; Shenoy, V. B.; Eda, G.; Chhowalla, M. *Nat. Mater.* **2013**, *12*, 850−855.

(6) Wang, H.; Lu, Z.; Xu, S.; Kong, D.; Cha, J. J.; Zheng, G.; Hsu, P.-C.; Yanb, K.; Bradshaw, D.; Prinz, F. B.; Cui, Y. *Proc. Natl. Acad. Sci. U.S.A.* **2013**, *110*, 19701.

(7) Huang, X.; Zeng, Z.; Bao, S.; Wang, M.; Qi, X.; Fan, Z.; Zhang, H. *Nat. Commun.* **2013**, *4*, 1444.

(8) Ma, C.-B.; Qi, X.; Chen, B.; Bao, S.; Yin, Z.; Wu, X.-J.; Luo, Z.; Wei, J.; Zhang, H.-L.; Zhang, H. *Nanoscale* **2014**, *6*, 5624.

(9) Benck, J. D.; Hellstern, T. R.; Kibsgaard, J.; Chakthranont, P.; Jaramillo, T. F. *ACS Catal.* **2014**, *4*, 3957.

(10) Merki, D.; Hu, X. L. *Energy Environ. Sci.* **2011**, *4*, 3878.

(11) Li, Y. G.; Wang, H. L.; Xie, L. M.; Liang, Y. Y.; Hong, G. S.; Dai, H. J. *J. Am. Chem. Soc.* **2011**, *133*, 7296.

(12) Liao, L.; Zhu, J.; Bian, X. J.; Zhu, L. N.; Scanlon, M. D.; Girault, H. H.; Liu, B. H. *Adv. Funct. Mater.* **2013**, *23*, 5326.

(13) Li, D. J.; Maiti, U. N.; Lim, J.; Choi, D. S.; Lee, W. J.; Oh, Y.; Lee, G. Y.; Kim, S. O. *Nano Lett.* **2014**, *14*, 1228.

(14) Yan, Y.; Xia, B. Y.; Qi, X. Y.; Wang, H. B.; Xu, R.; Wang, J. Y.; Zhang, H.; Wang, X. *Chem. Commun.* **2013**, *49*, 4884.

(15) Chang, Y. H.; Lin, C. T.; Chen, T. Y.; Hsu, C. L.; Lee, Y. H.; Zhang, W. J.; Wei, K. H.; Li, L. J. *Adv. Mater.* **2013**, *25*, 756.

(16) Ge, X.; Chen, L.; Zhang, L.; Wen, Y.; Hirata, A.; Chen, M. *Adv. Mater.* **2014**, *26*, 3100.

(17) Vrubel, H.; Merki, D.; Hu, X. L. *Energy Environ. Sci.* **2012**, *5*, 6136.

(18) Kibsgaard, J.; Jaramillo, T. F.; Besenbacher, F. *Nat. Chem.* **2014**, *6*, 248.

(19) Popczun, E. J.; McKone, J. R.; Read, C. G.; Biacchi, A. J.; Wiltrout, A. M.; Lewis, N. S.; Schaak, R. E. *J. Am. Chem. Soc.* **2013**, *135*, 9267.

(20) Faber, M. S.; Dziedzic, R.; Lukowski, M. A.; Kaiser, N. S.; Ding, Q.; Jin, S. *J. Am. Chem. Soc.* **2014**, *136*, 10053.

(21) Kong, D.; Wang, H.; Lu, Z.; Cui, Y. *J. Am. Chem. Soc.* **2014**, *136*, 4897.

(22) Vrubel, H.; Hu, X. L. *ACS Catal.* **2013**, *3*, 2002.

(23) Yu, Y. F.; Li, C.; Liu, Y.; Su, L. Q.; Zhang, Y.; Cao, L. Y. *Sci. Rep.* **2013**.

(24) Bockris, J. O. *Russ. J. Electrochem.* **1995**, *31*, 1211.

(25) Weber, T.; Muijsers, J. C.; Niemantsverdriet, J. W. *J. Phys. Chem.* **1995**, *99*, 9194.

(26) Chang, C. H.; Chan, S. S. *J. Catal.* **1981**, *72*, 139.

(27) Muller, A.; Jaegermann, W.; Enemark, J. H. *Coordin. Chem. Rev.* **1982**, *46*, 245.

(28) Lee, C.; Yan, H.; Brus, L. E.; Heinz, T. F.; Hone, J.; Ryu, S. *ACS Nano* **2010**, *4*, 2695.

(29) Yu, Y.; Huang, S.-Y.; Li, Y.; Steinmann, S. N.; Yang, W.; Cao, L. *Nano Lett.* **2014**, *14*, 553.

(30) Voiry, D.; Salehi, M.; Silva, R.; Fujita, T.; Chen, M. W.; Asefa, T.; Shenoy, V. B.; Eda, G.; Chhowalla, M. *Nano Lett.* **2013**, *13*, 6222.

(31) Xie, J. F.; Zhang, J. J.; Li, S.; Grote, F.; Zhang, X. D.; Zhang, H.; Wang, R. X.; Lei, Y.; Pan, B. C.; Xie, Y. *J. Am. Chem. Soc.* **2013**, *135*, 17881.